Measurements of the Young's modulus of hydroxide catalysis bonds, and the effect on thermal noise in ground-based gravitational wave detectors

Margot Phelps, Anna-Maria van Veggel, James Hough, Chris Messenger, David Hughes, William Cunningham, Karen Haughian, and Sheila Rowan

Phys. Rev. D **97**, 102004 — Published 11 May 2018

DOI: 10.1103/PhysRevD.97.102004

Measurements of the Young's modulus of hydroxide catalysis bonds, and the effect on thermal noise in ground-based gravitational wave detectors

Margot Phelps[1], Anna-Maria van Veggel[1], James Hough[1], Chris Messenger[1], David Hughes[2], William Cunningham[1], Karen Haughian[1], and Sheila Rowan[1]
1 *SUPA, School of Physics and Astronomy, The University of Glasgow, Glasgow, G12 8QQ, UK and*
2 *SUPA, Institute of Thin Films, Sensors, and Imaging, University of the West of Scotland, Paisley, UK*

With the outstanding results from the detection and observation of gravitational waves from coalescing black holes and neutron star inspirals, it is essential that pathways to further improve the sensitivities of the LIGO and VIRGO detectors are explored. There are a number of factors that potentially limit the sensitivities of the detectors. One such factor is thermal noise, a component of which results from the mechanical loss in the bond material between the silica fibre suspensions and the test mass mirrors. To calculate its magnitude, the Young's modulus of the bond material has to be known with reasonable accuracy. In this paper we present a new combination of ultrasonic technology and Bayesian analysis to measure the Young's modulus of hydroxide catalysis bonds between fused silica substrates. Using this novel technique, we measure the bond Young's modulus to be $18.5\pm^{2.0}_{2.3}$GPa. We show that by applying this value to thermal noise models of bonded test masses with suitable attachment geometries, a reduction in suspension thermal noise consistent with an overall design sensitivity improvement allows a factor of 5 increase in event rate to be achieved.

I. INTRODUCTION

In 2015, a gravitational wave (GW) signal from a binary black hole merger passed through the arms of the Advanced LIGO (aLIGO) interferometers, resulting in the first direct detection of gravitational waves [1]. This long-awaited detection of GWs made worldwide news one hundred years after Einstein first predicted them in 1916 [2]. Since then there have been four more binary black hole inspiral events, as well as the ground-breaking GW detection of a neutron star inspiral [3–7]. Requiring 50 years of technological development before the first detection, the extremely low amplitudes of GWs have always proved to be a challenge. To detect these signals, ground-based detectors like aLIGO and VIRGO need to be sensitive to changes in distance of close to 10^{-19} m [8] between freely suspended test masses spaced up to 4 km apart. Furthermore, for a detector to reliably measure such small displacement changes, it must be isolated as much as possible from all environmental effects that cause movement. Ground-based GW systems face an extensive list of fundamental and technical noise sources that limit their performance.

In particular the movement of particles driven by thermal energy, known as thermal noise, is a limiting noise source in ground-based detectors [9]. To mitigate this the optics, suspensions, and jointing material must all be constructed of low mechanical dissipation materials. This minimises the off-resonance thermal noise described by the Fluctuation Dissipation Theorem [10] that impacts detector sensitivity.

Hydroxide catalysis bonding (HCB), a method of creating chemical bonds between oxides or oxidisable materials with an aqueous hydroxide solution, has been the preferred technique for creating the necessary quasi-monolithic optic and suspension systems for current and future ground-based GW detectors [11–15]. This is due to the ability of HCBs to form strong, low noise, ultra-high vacuum compatible interfaces that are applicable both at room temperature [16] and cryogenic temperatures [17, 18]. These bonds are currently a core technology in all operating ground-based detectors, and as such their material properties have to be well understood. In particular the density, Poisson ratio, and Young's modulus are necessary to calculate thermal noise. The density of HCBs was calculated previously [19] and the Poisson ratio is inferred to be the same as fused silica. The Young's modulus proved to be challenging to characterise due to the bond being thin and in-accessible to use direct contact measurement approaches such as nano-indentation, which is used to determine the Young's modulus of other materials and coatings [20].

One measurement of a HCB's Young's modulus is available in the literature, a value of 7.9 GPa [21]. Here a bond was altered to make it artificially thick to allow for a nano-indentation measurement. This value has historically been used to determine thermal noise arising from the bonds for aLIGO [22].

As the sensitivity of detectors improves, it is necessary to attain more accurate values for the bond properties that directly contribute to the overall thermal noise of GW detectors. Thus a non-destructive technique for attaining Young's modulus values of hydroxide catalysis bonds is outlined in this paper, as well as the results and their impact on thermal noise budgets of Advanced LIGO and to the proposed aLIGO A+ upgrade [23].

II. THEORY OF ULTRASONIC MEASUREMENTS

The transmission and reflection of ultrasonic waves through materials can be used as a non-destructive

method of probing hidden properties [24]. This technology is explored here as a non-destructive means to determine the Young's modulus of HCBs.

An acoustic wave that passes from one medium to another can be expressed in terms of the acoustic impedance of each medium. The percentage of an incident wave reflected off a medium change from silica to air is given in Eq.1, where Z is the characteristic acoustic impedance of the medium passed through. $Z = \rho \cdot v$ where v is the acoustic velocity and ρ the density of the medium, we calculate $Z_{\text{air}} = 331.4$ m/s·1.225 kg/m^3 = 406 Rayls and $Z_{\text{silica}} = 5931$ m/s·2200 kg/m^3 = $13 \cdot 10^6$ Rayls

$$R_{\text{silica,air}} = \left| \frac{Z_{\text{air}} - Z_{\text{silica}}}{Z_{\text{silica}} + Z_{\text{air}}} \right| = \left| \frac{331.4 - 13 \cdot 10^6}{331.4 + 13 \cdot 10^6} \right| = 0.99 \tag{1}$$

This allows the assumption that the measured amplitude of the silica-to-air reflection of each sample is 99% of the incident wave, and is used as a proxy for the input signal.

An expression for an acoustic pulse reflected from a thin embedded layer that takes into account the layer thickness is needed to calculate the signal from the embedded HCB. To determine this value we follow the technique outlined in Physical Acoustics [25]. We derive an equation for R_{bond} from the complex pressure amplitudes of incident waves, $P_{\text{incident}} = Ae^{i(wt-kx)}$ and reflected waves, $P_{\text{reflect}} = Be^{i(wt+kx)}$. Applying acoustic impedance continuity boundary conditions at the start and end of the layer, $x = 0$ and $x = L$ the following equation is obtained

$$R_{\text{bond}} = \frac{i(\frac{Z_2}{Z_1} - \frac{Z_1}{Z_2}) \sin(k_2 L)}{2\cos(k_2 L) + i(\frac{Z_2}{Z_1} + \frac{Z_1}{Z_2}) \sin(k_2 L)} \tag{2}$$

The first and third mediums are both fused silica, $Z_1 = Z_3$. The second medium, the hydroxide catalysis bond, is represented by Z_2. L is the bond thickness and k_2 is the wave number of the bond medium.

We may use the approximation $L \to 0$ as the thickness of the bond, L, is of order 100 nm thick while the substrates are each 5 mm thick or more, $\sin(\text{k}_2\text{L}) \approx \text{k}_2\text{L}$ and $\cos(\text{k}_2\text{L}) \approx 1 - (\text{k}_2\text{L})^2/2$. This simplifies the equation to

$$R_{\text{bond}} = \frac{i(\frac{Z_2}{Z_1} - \frac{Z_1}{Z_2}) k_2 L}{2(1 - \frac{(k_2 L)^2}{2}) + i(\frac{Z_2}{Z_1} + \frac{Z_1}{Z_2}) k_2 L} \tag{3}$$

Assuming the density of HCBs and fused silica are the same, the impedance terms simplify to ratios of the Young's moduli, $\frac{Z_1}{Z_2} \approx \sqrt{(E_2/E_1)}$. The wave number k can also be expressed in terms of acoustic velocity and the frequency of the ultrasonic transducer, $k_2 = 2\pi/\lambda_2 = 2f\pi/v_2$. Additionally dropping L and L^2 terms in the denominator due to the small L values gives us

$$R_{\text{bond}} \approx i \left[\sqrt{\frac{E_2}{E_1}} - \sqrt{\frac{E_1}{E_2}} \right] \sqrt{\frac{\rho}{E_2}} \pi f L \tag{4}$$

For HCB values of L =7 µm, Eq.2-4 differ by < 2%. Eq.4 is used where L <100 nm, as R_{bond} is expressed only in terms of the variable of interest E_2 and of known or measured values E_1, ρ, pulse frequency f and HCB thickness, L.

III. EXPERIMENTAL METHOD

In this experiment an ultrasonic transducer with a centre frequency 12 MHz and a bandwidth of 6-15 MHz, was contacted with glycerine to one side of an HCB bonded fused silica doublet. A schematic of the set-up is shown in Fig. 1. As indicated in the schematic, the reflected

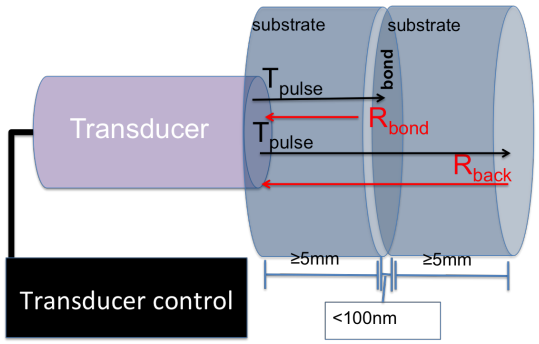

FIG. 1. Experiment schematic: The transducer sends out an ultrasonic pulse that travels through the fused silica sample on the right. Signals are reflected back from the embedded HCB and rear face of the silica sample, received by the same transducer and recorded.

signals were received back to the same transducer that sent the pulse. The amplitudes and phase of the reflected signals were recorded for each measurement on a 200 MHz oscilloscope and averaged 4096 times to attain the datasets shown in Fig.2. An un-bonded fused silica cylinder 12 mm long was measured as a calibration sample. The bonded samples were created by joining two 6 mm long fused silica discs together with a hydroxide catalysis bond in the middle, as shown in the schematic in Fig. 1. Six different bonded fused silica discs of this type were measured in this experiment. Acoustic data for one of the bonded samples is shown in Fig.2.

IV. BOND THICKNESS MEASUREMENTS

The reflection equation R_{bond} is linearly dependent on bond thickness L. To measure this directly, the bonded samples were cut into several slices perpendicular to the bond plane, polished and coated with gold (to reduce surface charging) then imaged in an FEI Nova 200 Dual beam FIB system scanning electron microscope (SEM), as in the left of Fig. 3.

All the SEM results were combined via linear interpolation to produce maps of each sample's HCB thickness,

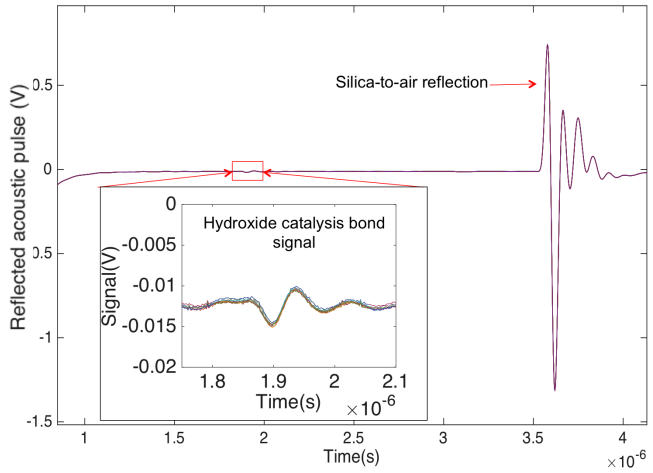

FIG. 2. Acoustic pulse reflection data of a hydroxide catalysis bonded fused silica sample. The signal reflected from the bond interface is shown in the middle, and the silica-to-air interface (i.e. input signal) on the right.

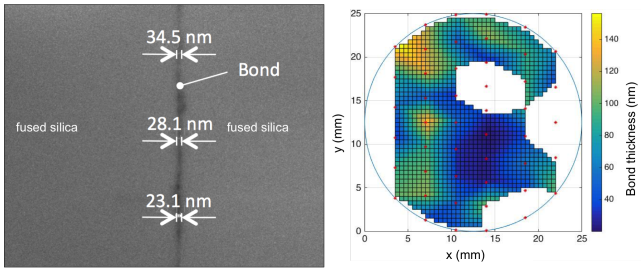

FIG. 3. Left: SEM image of the bond(vertical line) with polished fused silica on either side. Right: Surface map of combined bond thickness measurements across sample 1. Blank spaces are visible where the surface became too highly charged to measure.

as in the right of Fig. 3. This allowed a direct correlation of thickness to ultrasonic measurements made in the same location. The average bond thickness and standard deviation by measurement location is shown in Table I together with the the sample characteristics.

V. ANALYSIS

We perform a Bayesian analysis of the data in which the signal model, Eq.5, is a function of $R_{\rm bond}$, described by Eq.4. We also introduce time offset Δt representing the unknown start time of the bond signal with reference to t_0, an arbitrarily defined time near the center of the timeseries where we expect the bond signal to be.

Our noise model contains two main components. We estimate these noise component Power Spectral Densities (PSDs) from segments of data taken before and after the bond signal and averaged over all the datasets taken on the same sample and at the same sample position.

The first component is low frequency noise which was intrinsic to each sample and the sample location being analysed. We see the same realisation of this low frequency noise in repeated measurements of the same sample. This source could be attributed to the sample geometry. This component has a red spectrum, i.e. higher power at low frequencies.

The second noise component has an approximately white spectrum, i.e. uniform power in frequency, and it dominates the former noise component at high frequency. We assume that each measurement contains an independent noise realisation for this component, which could be attributed to electronics noise. We are able to account for the noise components independent of their source using this analysis model, as described in this section and shown in Figs. 4(a) and 4(b).

By averaging the timeseries data we subdue the high frequency noise and are able to estimate the low frequency noise PSD, $P^{\rm l}$. By subtracting the averaged timeseries from each dataset we are left with the white noise components from which we can estimate the white noise PSD, $P^{\rm w}$.

Since the effect of the low-frequency noise source is to introduce a repeatable low-frequency signal, we model this as an additional signal component with corresponding unknown parameters. The specific realisation of this noise within the bond signal is not known a-priori so we parameterise this noise signal in the frequency domain assuming that each discrete frequency bin has an unknown phase ϕ_k and a known amplitude governed by our estimated low frequency PSD. We use only the first 15 frequency bins since this is the region over which the low frequency noise power exceeds that of the white noise. These parameters are included in a Markov chain Monte Carlo (MCMC) analysis [26] and marginalised over, therefore accounting for the common low-frequency noise present in multiple measurements of the same sample.

Sample	Diameter x width (mm)	Average $L_{\rm bond}$ (nm)	Error (nm)
1(top)	25x12	56.8	33.3
1(bottom)	25x12	40.4	27.8
1(center)	25x12	31.8	10.4
1(left)	25x12	75.0	37.7
1(right)	25x12	71.0	22.5
2(center)	25x12	30.7	7.3
3(center)	25x12	35.5	8.7
4(center)	50x10	49.6	29.5
5(center)	50x24	57.1	12.0
6(center)	50x10	95.5	42.1

TABLE I. Dimensions, measured HCB thicknesses, and standard deviation of layer thickness of each of the six bonded samples and transducer measurement position.

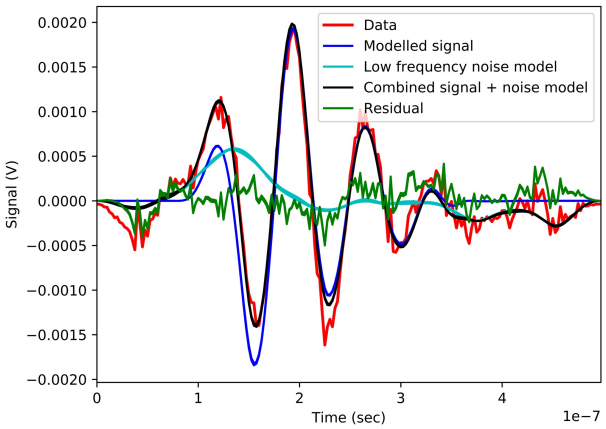

(a) Reflected bond signal and model components vs. time.

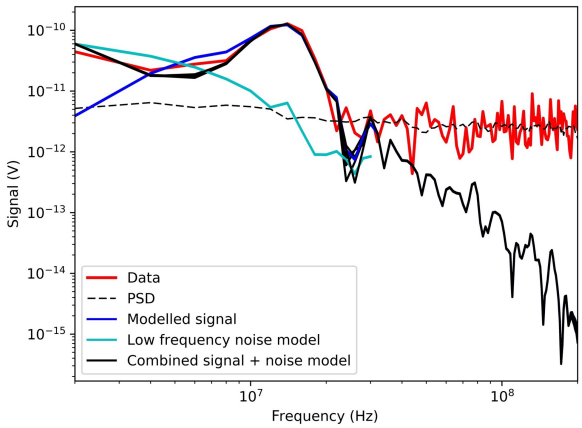

(b) Reflected bond signal and model components vs. frequency

FIG. 4. Time-domain and frequency-domain examples of the reflected bond signal and corresponding signal components are shown in Figs. 4(a) and 4(b). In both figures, the first term from our model Eq.5 is plotted in dark blue, shown with the common low frequency noise term, the second term in Eq.5 in cyan, the combined signal and noise models, $\tilde{s}$ in black. The measured data, $\tilde{b}$ is shown here in red. The residuals are also shown in dark green in Fig. 4(a). Each curve represents a set of curves drawn from the posterior distribution on the unknown parameters $R, dt, \vec{\phi}$.

Our signal model can be represented in the frequency domain by

$$\tilde{s}(f; R, \Delta t, \vec{\phi}) = \tilde{x} R i f e^{2\pi i f \Delta t} + \sum_{k=1}^{15} \frac{1}{2} \sqrt{N dt P_k^{\rm l}} e^{i\phi_k} \quad (5)$$

where $Rif = R_{\rm bond}$ from Eq.4, the discrete Fourier transform of the input pulse timeseries data is defined by $\tilde{x}$, the frequency is defined as f, the time offset is Δt, the timeseries sampling interval is dt, and the number of samples in the input signal timeseries is N.

We use uniform prior probability distributions on the parameters t_0, $R_{\rm bond}$, and noise phases $\vec{\phi}$ with the following limits. The start time t_0 ranges between 0 and 0.5 s, and is long enough to fully encompass the reflected pulse signal. The noise phases each ranged from 0 to 2π and $R_{\rm bond}$ ranges between 0 and an amplitude corresponding to the maximum allowed E_2 value. Since the bond is a silicate material it should not exceed the Youngs modulus of fused silica, 72 GPa. The measured HCB thicknesses and associated statistical error are interpreted as a Gaussian prior for L in which the measured value and the uncertainties represent the mean and standard deviation of the Gaussian respectively.

The likelihood function, based on a Gaussian noise model, is defined as

$$p(\tilde{b}|R, \Delta t, \vec{\phi}) = \prod_m \prod_{k=0}^{N-1} \frac{2}{\pi N dt P_{mk}^w} \exp\left(-\frac{|\tilde{b}_{mk} - \tilde{s}_{mk}|^2}{N dt P_{mk}^w} \right) \quad (6)$$

where m indexes over sets of measurements for which the sample and sample location were the same. The quantity $\tilde{b}$ is the Fourier transform of the measured reflected bond signal.

After performing an MCMC analysis to obtain samples from the posterior probability distribution on the quantity R, we combine this with our knowledge of the bond thickness L to generate the posterior on the Youngs modulus of HCBs, E_2. This is done using

$$p(E_2|\tilde{b}) \propto \sum_j^n p(L = L(E_2, R_j)) \left| \frac{dL}{dE_2} \right| \quad (7)$$

where the sum is over posterior R samples and the derivative is the Jacobian required to transform the integral over bond thickness L into one over E_2. This derivative and the function $L(E_2, R)$ are obtained via Eq.4.

A time-domain example of the reflected bond signal and corresponding signal and components is shown in Fig. 4(a). The sum of the model and low frequency common noise component, s, match the measured reflection signal with residuals consistent with those expected from the white noise PSD. In Figure 4(b) the strength of the bond signal against the noise background can be seen in the frequency domain.

Finally a posterior on the Youngs modulus of the bonds, E_2, is obtained from each group of measured samples and is shown in Fig. 5. These posteriors are statistically independent and therefore their product is used to obtain an improved result. All input posteriors are broadly consistent and the final posterior has support from all inputs. Despite the apparent spread seen in the posterior distributions they all share common support for the region under the final combined posterior. Thus we obtain a best estimate value with a 90% confidence range of $18.5 \pm^{2.0}_{2.3}$GPa for the Youngs modulus of hydroxide catalysis bonds.

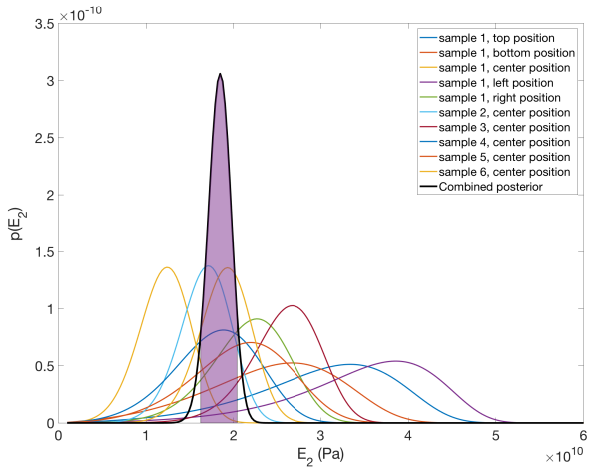

FIG. 5. Individual E_2 posteriors of each measured sample. The final combined posterior is shown in black and a 90% confidence level is shown in blue.

VI. IMPACT ON THE THERMAL NOISE OF GW DETECTORS

Thermal noise affects instrument sensitivity across its most sensitive frequency band, 10-100 Hz [27]. The new Young's modulus value was used to assess the bond's contribution to thermal noise of GW detectors.

This approach utilised Levin's method [28] to calculate thermal noise as previously used by Cunningham et al [22], who published a figure of $5.4 \cdot 10^{-22}\mathrm{m}/\sqrt{\mathrm{Hz}}$. Re-evaluating these aLIGO models using the updated value of 18.5 GPa for the HCB Young's modulus gives a new value of $5.8 \cdot 10^{-22}\mathrm{m}/\sqrt{\mathrm{Hz}}$.

Although this represents a 7% increase in the estimated excess thermal noise associated with the bonds, both the original and re-calculated values are below the aLIGO thermal noise budget level of $7 \cdot 10^{-22}\mathrm{m}/\sqrt{\mathrm{Hz}}$ [29]. Future detectors and detector upgrades will have different test mass materials, geometries, operating temperatures, and more stringent thermal noise requirements. In these cases estimating the bond's thermal noise contribution as accurately as possible becomes much more important to ensure this technology continues to meet detector design requirements. One example of this is addressed in the following section, for a bonded test mass geometry that is suitable for a potential upgrade to aLIGO.

A. A+ aLIGO upgrade ear design and FE thermal noise analysis

A+, an incremental upgrade to existing aLIGO detectors is currently being developed. This upgrade will make use of existing aLIGO infrastructure and technologies and aims for a 1.7x increase in range over aLIGO, using the binary neutron star inspirals as a benchmark[23]. In order to meet the sensitivity required for A+ a few key parameters are revisited. The coating thermal noise budget is proposed to be half of aLIGO, utilising improvements to coating technologies. The use of frequency dependent squeezing is also proposed to lower the quantum noise level. With the successful implementation of the planned upgrades, the A+ design strain sensitivity curve would improve enough attain the 1.7x increase in range over aLIGO.

This increase in range demands a higher detector sensitivity and thus a lower bond thermal noise budget of $4 \cdot 10^{-22}\mathrm{m}/\sqrt{\mathrm{Hz}}$, based on a technical noise budget of 10% of the total thermal noise at 100 Hz. Here we investigate an updated ear design for the A+ upgrade, with the aim of further reducing the bond's contribution to detector thermal noise to meet the requirements of the upgrade. The most straightforward way of doing this was to reduce the surface area of the bonds by reducing the size of the ears on the masses, in comparison to the original aLIGO ear design [30]. This was done by going from two ears per mass to four ears. The ears are positioned on the mass so that the horns are the same distance away from each other as they are in aLIGO, now with a space between two ears instead of a single long ear. This and an angled ear geometry allow for a reduction in area of 34%, while keeping a wide margin of safety in terms of stress on the ear and bonds.

A few different geometries of new ears were investigated. A small, angled ear was selected as the best combination of lower thermal noise, bond strength, and safe deformation of the ear horns under load as shown on the right of Fig. 6. In this design two ears are positioned on both sides of an A+ mass, keeping the horn separation the same as aLIGO, with a space between two smaller ears instead of the long single aLIGO ear, as shown on the left in Fig. 6.

To understand how the new HCB Young's modulus

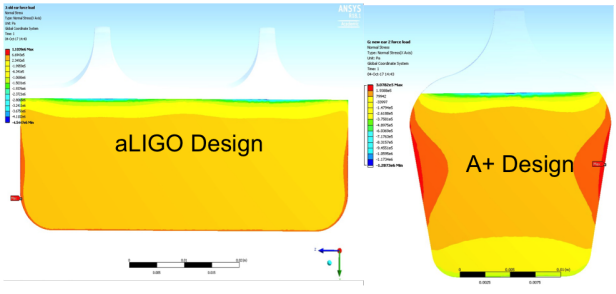

FIG. 6. Comparisons of ear design geometries for aLIGO and A+

affects noise levels, we have modelled the thermal noise contribution of the new bonded ear design in Figure 6 and compared it to a proposed A+ sensitivity curve. This A+ ear design offers smaller ears while keeping similar stresses and horn deformation under gravity to the aLIGO design. The horn separation and standoff distance from the test mass also remain the same as the

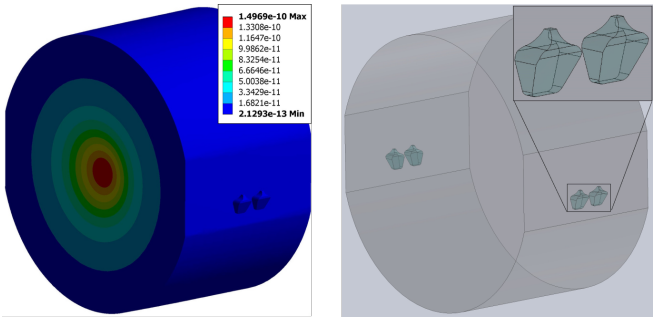

FIG. 7. FE model of an A+ bonded test mass, with the new 4 ear design

aLIGO ears. Additionally, this design keeps a safety factor of 3 in the bond's tensile maximum normal stress, a factor based on the ratio of average tensile strength of HCBs, 16 MPa, and the maximum normal tensile stress in the bond, 5.2 MPa, taking into account a test mass load of 40 kg and an ear area that is 34% less per mass then aLIGO ears.
The FE model of the selected ear design bonded onto a A+ test mass is shown in Fig. 7. A comparison of the values calculated from the ANSYS models of bonded masses for aLIGO and aLIGO A+ is outlined in Table II.

Parameter of bond per test mass	aLIGO	A+
Horn deformation under gravity (µm)	0.67	0.69
Max equivalent stress under gravity (MPa)	9.2	9.3
Max tensile stress, normal (MPa)	2.7	5.2
Max tensile stress, shear (MPa)	±3.5	±4.8
Thermal noise, required ($\cdot 10^{-22}\mathrm{m}/\sqrt{\mathrm{Hz}}$)	7	4
Thermal noise, modelled ($\cdot 10^{-22}\mathrm{m}/\sqrt{\mathrm{Hz}}$)	5.8	3.8

TABLE II. Comparison of aLIGO and aLIGO A+ ear design parameters from FE models

The calculated thermal noise of the new ear design, which assumes a bond thickness of 61 nm, was therefore calculated from the model to be $3.8 \cdot 10^{-22}\mathrm{m}/\sqrt{\mathrm{Hz}}$. This meets the projected A+ thermal noise requirement of $4 \cdot 10^{-22}\mathrm{m}/\sqrt{\mathrm{Hz}}$.

VII. DISCUSSION AND CONCLUSIONS

A new combination of ultrasonic technology and Bayesian analysis that measured the material properties of extremely thin layers embedded in brittle substrates has been presented here. A best estimate value of the Young's modulus of hydroxide catalysis bonds of $18.5\pm^{2.0}_{2.3}$GPa with a 90% confidence range was attained. This new value was used to find an aLIGO bond thermal noise of $5.8 \pm 0.6 \cdot 10^{-22}\mathrm{m}/\sqrt{\mathrm{Hz}}$, which meets the aLIGO bond thermal noise requirement of $7 \cdot 10^{-22}\mathrm{m}/\sqrt{\mathrm{Hz}}$. A new bonded ear design is presented for the next GW detector upgrade, A+. This design has a thermal noise for a bonded A+ test mass calculated here to be $3.8 \cdot 10^{-22}\mathrm{m}/\sqrt{\mathrm{Hz}}$, which meets an A+ thermal noise design requirement of $4 \cdot 10^{-22}\mathrm{m}/\sqrt{\mathrm{Hz}}$. This indicates that hydroxide catalysis bonds continue to be a good choice for the construction of quasi-monolithic suspensions in GW detectors. In an era of gravitational wave astronomy where the detector sensitivities are pushed ever lower and cryogenic technologies are proposed, we will next use the analysis presented here to probe the material properties of bonded materials suitable for future cryogenic detectors, such as sapphire and silicon.

VIII. ACKNOWLEDGMENTS

The authors would like to thank the UK Science and Technology Facilities Council (Grant numbers ST/I001085/1, ST/J000361/1, ST/L000946/1, ST/N005422/1), the University of Glasgow, the Scottish Funding Council and the Royal Society, A. A. van Veggel is the holder of a Royal Society Dorothy Hodgkin Fellowship, grant number DH12001, for financial support. We would like to express our gratitude to our colleagues in the GEO600 and LIGO Scientific Collaboration for their interest in this area. The authors gratefully acknowledge the support of the United States National Science Foundation (NSF) for the construction and operation of the LIGO Laboratory and Advanced LIGO as well as the Science and Technology Facilities Council (STFC) of the United Kingdom, the Max-Planck Society (MPS), and the State of Niedersachsen/Germany for support of the construction of Advanced LIGO and construction and operation of the GEO600 detector. Additional support for Advanced LIGO was provided by the Australian Research Council. The authors would also like to thank Norna Robertson and Matt Abernathy for their helpful reviews. LIGO-DOCUMENT-P1700423.

[1] B. P. Abbott, others (the LIGO Scientific Collaboration, and VIRGO Collaboration). Observation of gravitational waves from a binary black hole merger. *Physical Review Letters*, 2016.

[2] A. Einstein. Die Grundlage der allgemeinen Relativitätstheorie. *Annalen der Physik*, 354(7):769–822, 1916.

[3] B. P. Abbott, others (the LIGO Scientific Collaboration, and VIRGO Collaboration). Gw151226: Observation of gravitational waves from a 22 solar mass binary black hole coalescence. *Physical Review Letters*, 2016.

[4] B. P. Abbott, others (the LIGO Scientific Collaboration, and VIRGO Collaboration). Gw170104: Observation of 50 solar mass binary black hole coalescence at redshift 0.2. *Physical Review Letters*, 2017.

[5] B. P. Abbott, others (the LIGO Scientific Collaboration, and VIRGO Collaboration). Gw170814: A three-detector observation of gravitational waves from a binary black hole coalescence. *Physical Review Letters*, 2017.

[6] B. P. Abbott, others (the LIGO Scientific Collaboration, and VIRGO Collaboration). Gw170817: Observation of gravitational waves from a binary neutron star inspiral. *Physical Review Letters*, 2017.

[7] B. P. Abbott, others (the LIGO Scientific Collaboration, and VIRGO Collaboration). Gw170608: Observation of a 19-solar-mass binary black hole coalescence. *Astrophysical Journal Letters*, 2017.

[8] P.R. Saulson. *Fundamentals of Interferometric Gravitational Wave Detectors*. World Scientific, 1994.

[9] Massimo Bassan, editor. *Advanced Interferometer and the Search for Gravitational Waves*, volume 404. Springer, 2014.

[10] H. B. Callen and T. A. Welton. Irreversibility and generalized noise. *Phys. Rev. 83, 34*, 1951.

[11] Harald Luck et al. The upgrade of geo600. In *Gravitational waves. Proceedings, 8th Edoardo Amaldi Conference, Amaldi 8, New York, USA, June 22-26*, 2009.

[12] C Affeldt et al. Advanced techniques in geo 600. *Classical and Quantum Gravity*, 27(084003), 2014.

[13] F Acernese et al. Advanced virgo: a second-generation interferometric gravitational wave detector. *Classical and Quantum Gravity*, 2014.

[14] G. M. Harry and the LIGO Scientific Collaboration. Advanced ligo: the next generation of gravitational wave detectors. *Classical and Quantum Gravity*, 27(8):084006, 2010.

[15] Yoichi Aso and others (the KAGRA Collaboration). Interferometer design of the kagra gravitational wave detector. *Physical Review D*, 2013.

[16] D. H. Gwo. Ultra precise and reliable bonding method: Us6284085B1, 2001.

[17] R. Douglas, A. A. van Veggel, L. Cunningham, K. Haughian, J. Hough, and S. Rowan. Cryogenic and room temperature strength of sapphire jointed by hydroxide-catalysis bonding. *Classical and Quantum Gravity*, 31 (045001), 2014.

[18] N. Beveridge, A. A. van Veggel, M. Hendry, P. Murray, R. A. Montgomery, E. Jesse, J. Scott, R. B. Bezensek, L. Cunningham, J. Hough, R. Nawrodt, S. Reid, and S. Rowan. Low-temperature strength tests and sem imaging of hydroxide catalysis bonds in silicon. *Classical and Quantum Gravity*, 2011.

[19] Karen Haughian. *Aspects of Materials Research for Advanced and Future Generations of Gravitational Wave Detectors*. PhD thesis, University of Glasgow, 2011.

[20] M. R.Abernathy. *Mechanical Properties of Coating Materials for Use in the Mirrors of Interferometric Gravitational Wave Detectors*. PhD thesis, University of Glasgow, 2012.

[21] E. J. Elliffe. *Aspects of Thermal Noise Modeling in Ground-Based Gravitational Wave Detetors and Developments of Hydroxide Catalysis Bonding for Space-Based Gravitational Wave Detectors and other Optical Applications*. PhD thesis, University of Glasgow, 2005.

[22] L. Cunningham, P.G. Murray, A. Cunningham, E.J. Elliffe, G.D. Hammond, and K. Haughian. Re-evaluation of the mechanical loss factor of hydroxide-catalysis bonds and its significance for the next generation of gravitational wave detectors. *Physics Letters A*, 2010.

[23] M. Zucker. Private communication.

[24] Emmanuel P. Papadakis, editor. *Ultrasonic Instruments & Devices*. Academic Press, 1999.

[25] L. Kinsler et al. *Fundamentals of Acoustics 4^{th} Edition*. Wiley, 2000.

[26] D. Foreman-Mackey, D. Hogg, D. Lang, and J. Goodman. emcee: The mcmc hammer. *Publications of the Astronomical Society of Pacific, Volume 125, Issue 925, pp. 306*, 2013.

[27] S Hild, H Grote, J Degallaix, S Chelkowski, K Danzmann, A Freise, M Hewitson, J Hough, H Lück, M Prijatelj, et al. DC-readout of a signal-recycled gravitational wave detector. *Classical and Quantum Gravity*, 26(5): 055012, 2009.

[28] Yu. Levin. Internal thermal noise in the ligo test masses: A direct approach. *Physical Review D*, 1998.

[29] P. Fritschel, D. Coyne, et al. T010075 advanced ligo systems design. Technical report, 2009.

[30] S. M. Aston, M. A. Barton, A. S. Bell, N. Beveridge, B. Bland, A. J. Brummitt, G. Cagnoli, et al. Update on quadruple suspension design for advanced ligo. *Classical and Quantum Gravity*, 2012.